

Electronic Supplementary Information

Enhanced syngas production from CO₂ photoreduction over CoPd alloys modified NiAl-LDH under visible light

Lan Yang,^{‡^a} Lei Li,^{‡^a} Pengfei Xia,^a Huiyi Li,^a Jingjing Yang,^a Xiaohong Li,^a Xiaodi Zeng,^a Xiaodong Zhang,^a Chong Xiao^{*^{ab}} and Yi Xie^{ab}

a. Hefei National Laboratory for Physical Sciences at the Microscale, CAS Center for Excellence in Nanoscience, University of Science and Technology of China, Hefei, Anhui, 230026, P. R. China.

b. Institute of Energy, Hefei Comprehensive National Science Center, Hefei, Anhui, 230031, P. R. China. Email: cxiao@ustc.edu.cn.

[‡] These authors contributed equally to this work.

Experimental Section

Methods

Materials. Ni(NO₃)₂ · 6H₂O, Al(NO₃)₃ · 9H₂O, hexamethylenetetramine (HMT), and K₃[Co(CN)₆] were purchased from Sigma-Aldrich Co., Ltd. and Na₂PdCl₄ was purchased from Shanghai Aladdin Biochemical Technology Co., Ltd. The aforementioned reagents were all of the analytical grade and used without further purification.

Synthesis of NiAl-LDH. The NiAl-LDH was synthesized referred to Sasaki's method¹. 93.75 mM Ni(NO₃)₂ · 6H₂O, 31.25 mM Al(NO₃)₃ · 9H₂O, and 131.25 mM HMT were dissolved in 40 mL of deionized water. The mixture was then heated in an autoclave at 140 °C for 24 h. The product was centrifuged and washed with water and ethanol, and finally dried at 60 °C overnight.

Synthesis of NiAl-LDH-Pd. The NiAl-LDH-Pd was synthesized referred to Zeng's method². The obtained NiAl-LDH (100 mg) were dispersed in 30 mL of deionized water by ultrasonication, then a certain amount of Na₂PdCl₄ was added and stirred for 3 h. The product was collected by centrifugation, washed with water, and redispersed in 30 mL of deionized water. Then a freshly prepared aqueous solution of NaBH₄ (20 × 10⁻³ M) was added and stirred for another 12 h. The final product was collected, washed with deionized water and ethanol in sequence, and dried at 60 °C overnight.

Synthesis of NiAl-LDH-CoPd. The NiAl-LDH-CoPd was synthesized referred to Zeng's method². The obtained NiAl-LDH (100 mg) were dispersed in 30 mL of deionized water by sonication, then a certain amount of then a certain amount of K₃[Co(CN)₆] was added and stirred for 3h, thereafter, a certain amount of Na₂PdCl₄ was added and stirred for another 3 h. The above obtained product was redispersed in 30 mL of deionized water. Then the freshly prepared aqueous solution of NaBH₄ (20 × 10⁻³ M) was added into the suspension and the resultant reaction mixture was stirred for 12 h. The final product was collected, washed with deionized water and ethanol in sequence, and dried at 60 °C overnight.

Characterizations. The X-ray diffraction (XRD) patterns were recorded on a Philips X'Pert Pro Super diffractometer with Cu K α radiation ($\lambda = 1.54178 \text{ \AA}$). The Scanning electron microscopy (SEM) images were by GeminiSEM 450. The transmission electron microscopy (TEM) images were obtained using Hitachi-7650 operated at an acceleration voltage of 100 kV. The high-resolution TEM (HRTEM), high-angle annular dark-field scanning TEM (HAADF-STEM), and corresponding energy-dispersive X-ray spectroscopy (EDS) line scan images were carried out on Talos F200X with an accelerating voltage of 200 kV. The high-angle annular dark-field scanning TEM (HAADF-STEM), and corresponding energy-dispersive X-ray spectroscopy (EDS) mapping images were carried out on JEOL JEM-F200 with an accelerating voltage of 200 kV. The nuclear magnetic resonance (1H-NMR) spectra were carried out on a Bruker AVANCE AV III 400 NMR spectrometer. The X-ray photoelectron spectroscopy (XPS) spectra were collected on an ESCALAB 250Xi with Mg K α (h $\nu = 1,253.6 \text{ eV}$) as the excitation source. And the XPS spectra were calibrated

against C1s at 284.8 eV. The ultraviolet-visible diffuse reflectance spectra (UV-vis DRS) were recorded on a PerkinElmer Lambda 950 UV-vis-NIR spectrophotometer.

The electrochemical-related characterizations were measured at the CHI760 electrochemical workstation (Shanghai Chenhua, China). For the photocurrent response test, 1 mg of sample was dispersed in 1 mL anhydrous ethanol and then evenly ground to slurry. The slurry was spread onto FTO glass with an area of 1 cm². The prepared FTO/sample was used as the working electrode with 0.5 M Na₂SO₄ aqueous solution as the electrolyte, saturated Ag/AgCl and Pt foil were used as the reference electrode and the counter electrode, respectively. The light source was a 300 W Xe-lamp. Mott-Schottky test was also carried out in Na₂SO₄ solution (0.5 M).

Photocatalytic CO₂ reduction measurements. Photocatalytic CO₂ reduction measurements were carried out in a closed Pyrex reaction vial using a 300 W Xe lamp (CEL-HXF300, Beijing China Education Au-light Co., Ltd.) with an optical cut-off filter ($\lambda > 420$ nm). Normally, 5 mg photocatalyst was dispersed in a 5 mL mixed solution of H₂O: CH₃CN: TEOA = 1 : 3: 1 (v/v/v), and then 2 μ mol Ru(bpy)₃Cl₂ 6H₂O was added. Before irradiation, continuous ventilation by high purity CO₂ gas was carried out. After reaction for 1h, the temperature of the reaction was tested to be about 40°C. The amount of evolved gaseous product was determined by Agilent GC-7890 equipped with TCD and FID detectors.

Determination of apparent quantum efficiency (AQE)

The apparent quantum efficiency (AQE) was measured using the same experimental apparatus for the photocatalytic CO₂ reduction, but with additional bandpass filters to obtain approximate monochromatic light at $\lambda = 420, 450, 475, 500$ nm. The power density was measured using a calibrated irradiance recorder (Perking Normal University Optical Instrument Factory) and the AQE was calculated by the following equation. The irradiation area was 8.1 cm². The average light intensities were measured to be 140, 175, 179, and 170 mW cm⁻², respectively. The AQE was calculated through the following equation:

$$AQE_{CO} = \frac{N_e}{N_p} = \frac{N_{CO}}{N_p} = \frac{2 * n_{CO} * N_A}{\frac{W * A * t}{h * \nu}} * 100\%$$

$$AQE_{H_2} = \frac{N_e}{N_p} = \frac{N_{H_2}}{N_p} = \frac{2 * n_{H_2} * N_A}{\frac{W * A * t}{h * \nu}} * 100\%$$

where N_e , N_p , N_{CO} , and N_{H_2} represent the number of reacted electrons, incident photons, generated CO and generated H₂, respectively; n_{CO} represents the molar number of generated CO, n_{H_2} represents the molar number of generated H₂; ν , W , A , and t are the incident light frequency, intensity, irradiation area, and time, respectively; N_A and h are the Avogadro's constant and Planck constant, respectively.

Density functional theory (DFT) calculation

The present first principle DFT calculations are performed by Vienna Ab initio Simulation Package (VASP)³ with the projector augmented wave (PAW) method⁴. The exchange-functional is treated using the generalized gradient approximation (GGA) of Perdew-Burke-Ernzerhof (PBE)⁵ functional. The energy cutoff for the plane-wave basis expansion was set to 450 eV and the force on each atom less than 0.02 eV/Å was set for the convergence criterion of geometry relaxation. Pd₁₃ and Co₆Pd₇ clusters were adopted to simulate the Pd-based and Co-Pd alloy photocatalyst, respectively. More than 15 Å vacuum was added along the z-direction to avoid the interaction between periodic structures for all systems. The Brillouin zone integration was performed using 2×2×1 k-point. The self-consistent calculations apply a convergence energy threshold of 10⁻⁵ eV. The adsorption energy E_{ads} was calculated according to

$$E_{ads} = E_{total} - E_{sub} - E_{mol}$$

where E_{total} is the total energy of the adsorbed system, E_{sub} and E_{mol} are the energies of the substrate and the adsorbate, respectively.

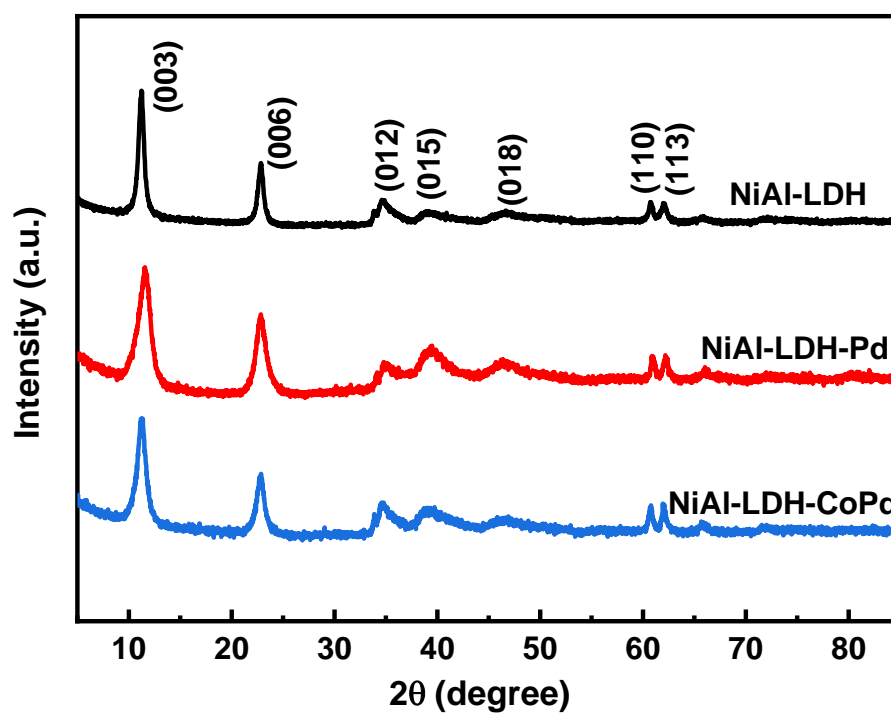


Fig. S1 The XRD patterns of the synthesized NiAl-LDH, NiAl-LDH-Pd, NiAl-LDH-CoPd.

The X-ray diffraction (XRD) patterns show diffraction peaks appear mainly at 11.1°, 22.7°, 34.8°, 39.3°, 47.0°, 60.7°, and 62.0°, which corresponding to the (003), (006), (012), (015), (018), (110), and (113) lattice planes, respectively, indexed to the NiAl-LDH (JCPDS No.015-0087).

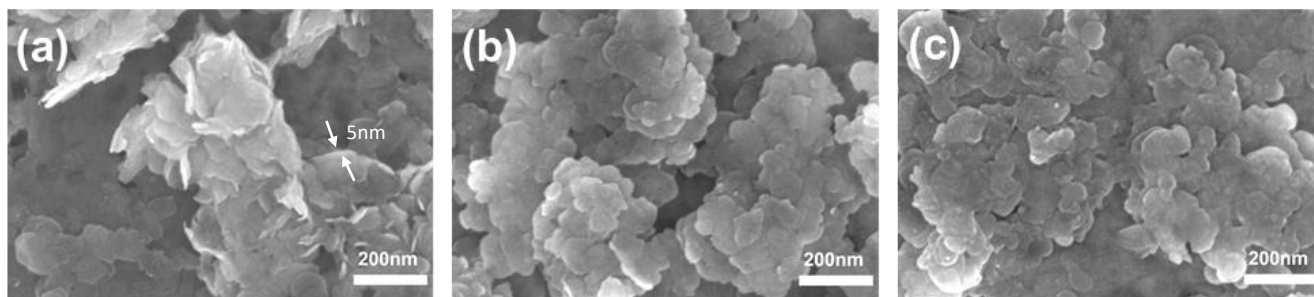


Fig. S2 SEM images of (a) NiAl-LDH, (b) NiAl-LDH-Pd, (c) NiAl-LDH-CoPd.

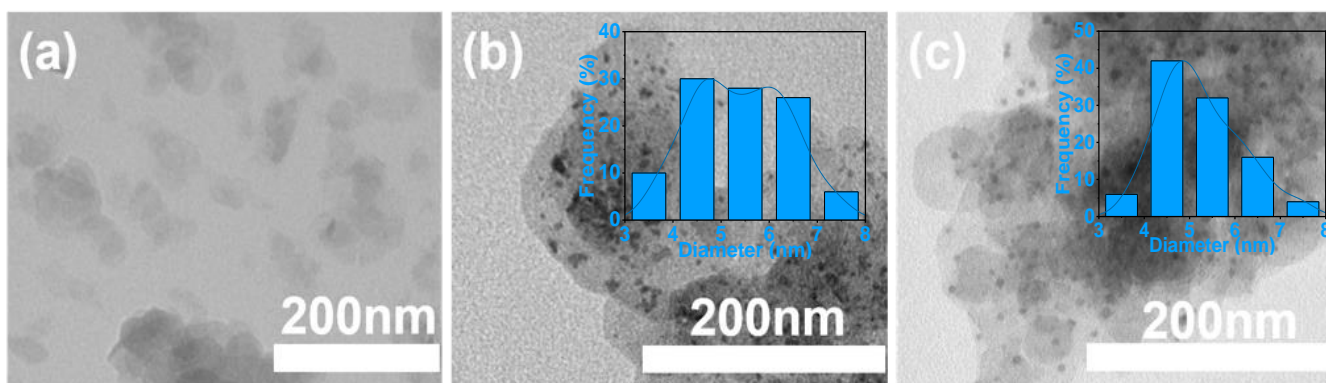


Fig. S3 TEM images of (a) NiAl-LDH, (b) NiAl-LDH-Pd, (c) NiAl-LDH-CoPd

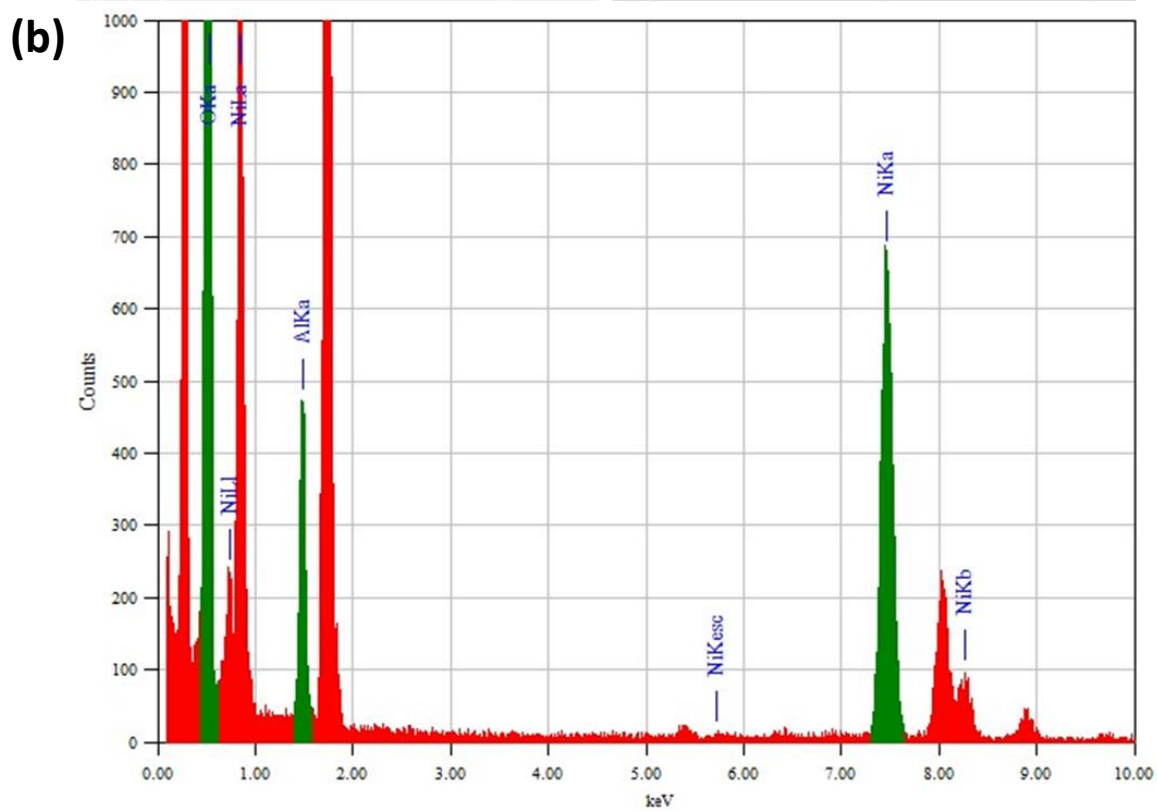
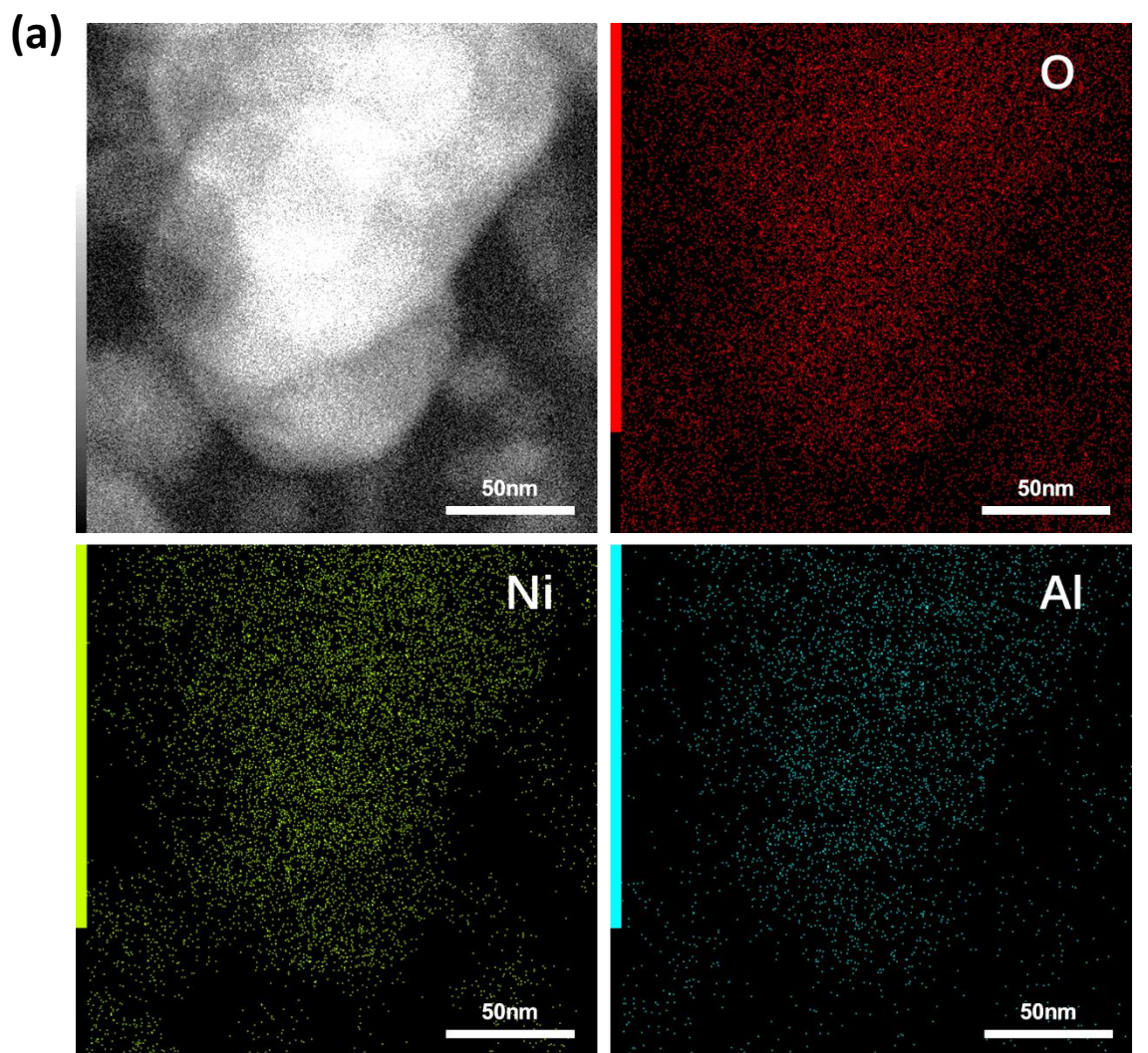


Fig. S4 (a) HAADF-STEM image and corresponding EDS mapping profiles of NiAl-LDH; (b) Energy-dispersive X-ray spectroscopy (EDS) of NiAl-LDH.

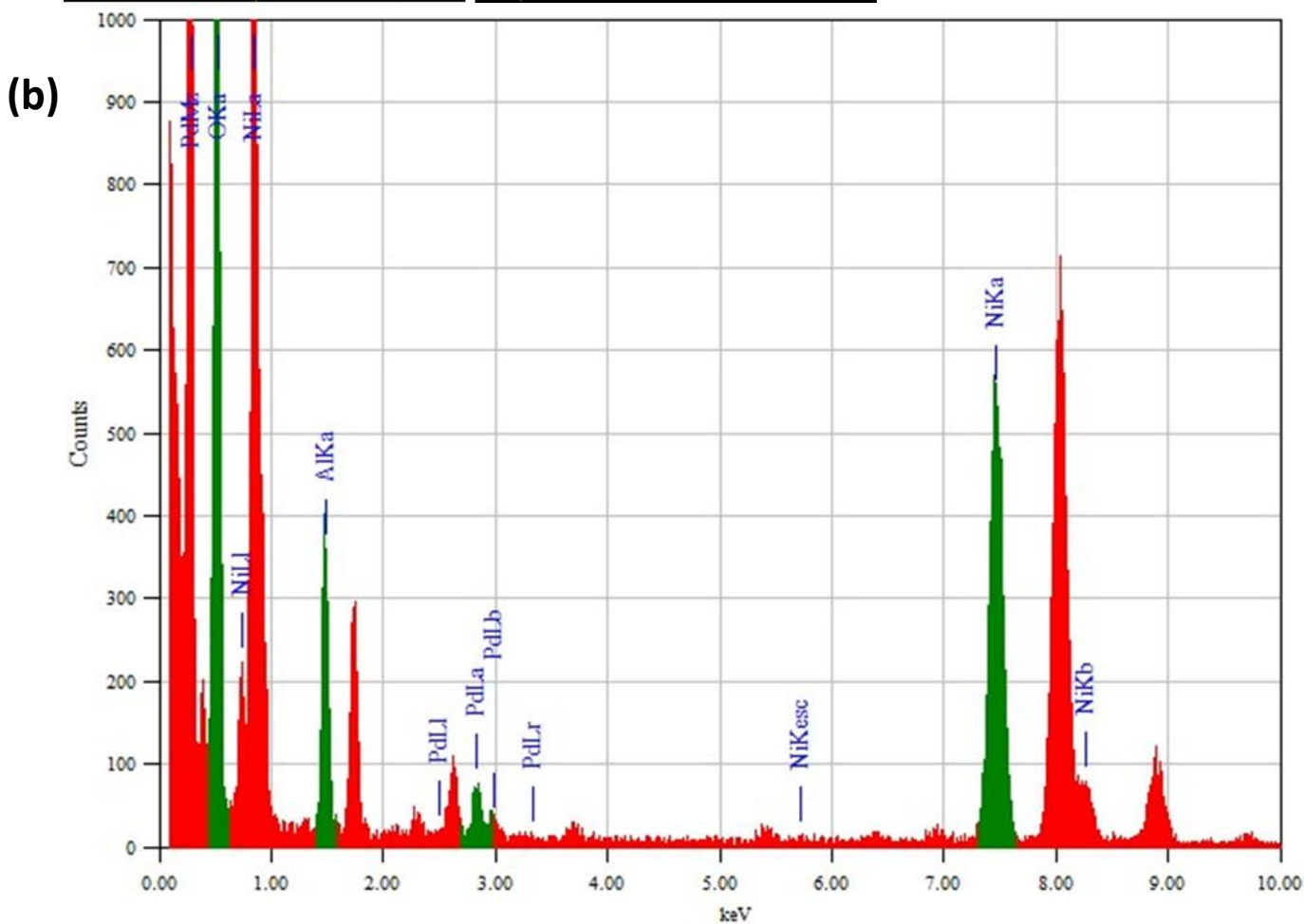
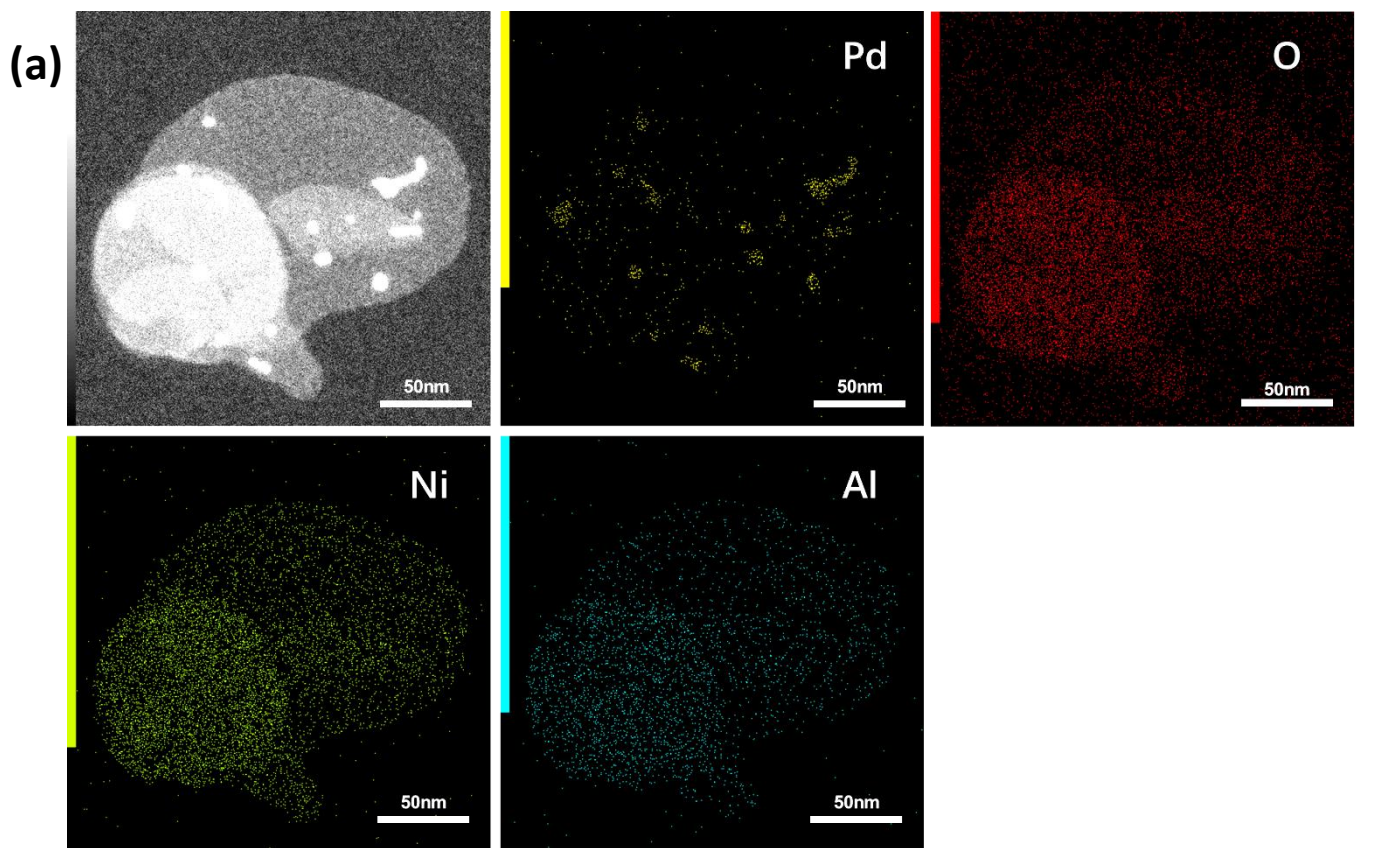


Fig. S5 (a) HAADF-STEM image and corresponding EDS mapping profiles of NiAl-LDH-Pd;
 (b) Energy-dispersive X-ray spectroscopy (EDS) of NiAl-LDH-Pd.

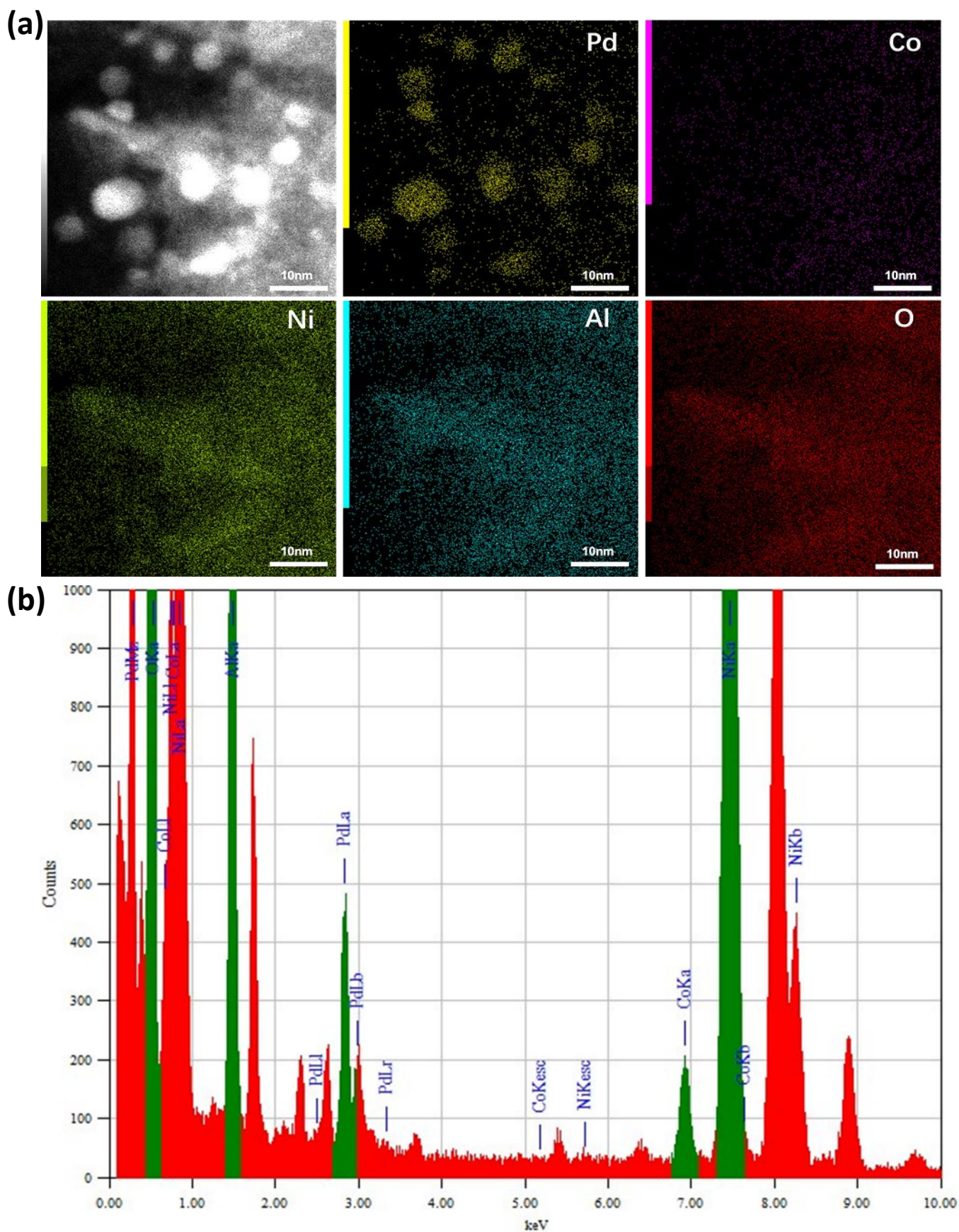


Fig. S6 (a) HAADF-STEM image and corresponding EDS mapping profiles of NiAl-LDH-CoPd; (b) Energy-dispersive X-ray spectroscopy (EDS) of NiAl-LDH-CoPd. Note: Due to the signal positions of Co K line and Ni K line are close, the EDS mapping profile of Co is interfered by Ni, but the Co Ka line in (b) shows the existence of Co.

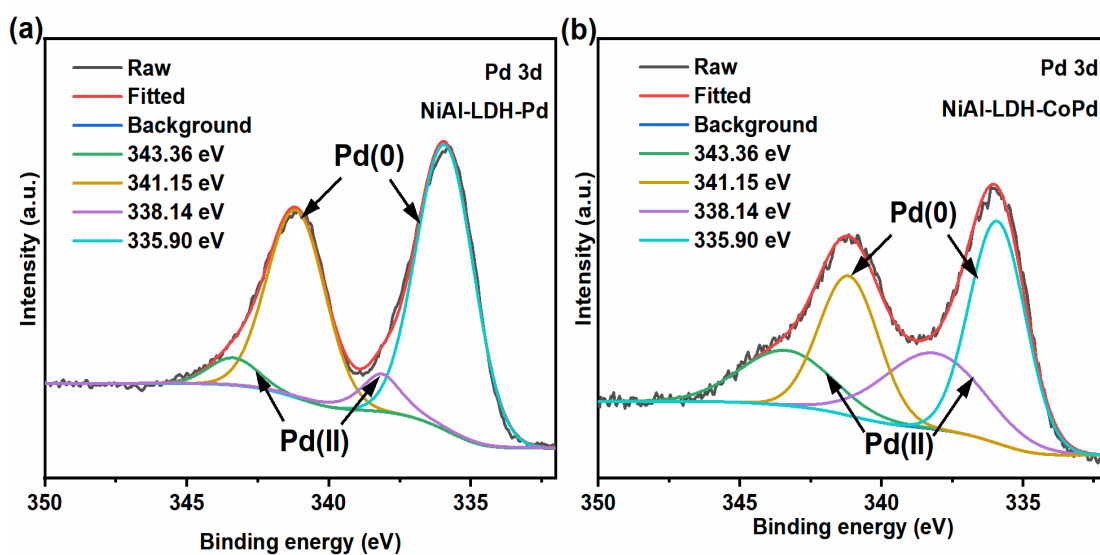


Fig. S7 High resolution XPS spectra of Pd 3d in (a) NiAl-LDH-Pd, (b) NiAl-LDH-CoPd.

The results of X-ray photoelectron spectroscopy (XPS) show that Pd 3d spectrum display four peaks in both NiAl-LDH-Pd (Fig. S7a, ESI†) and NiAl-LDH-CoPd (Fig. S7b, ESI†). The peaks at around 341.15 eV (Pd 3d_{3/2}) and 335.90 eV (Pd 3d_{5/2}) can be ascribed to Pd(0) species, and the peaks at 343.36 eV (Pd 3d_{3/2}) and 338.14 eV (Pd 3d_{5/2}) can be assigned to Pd(II).⁶

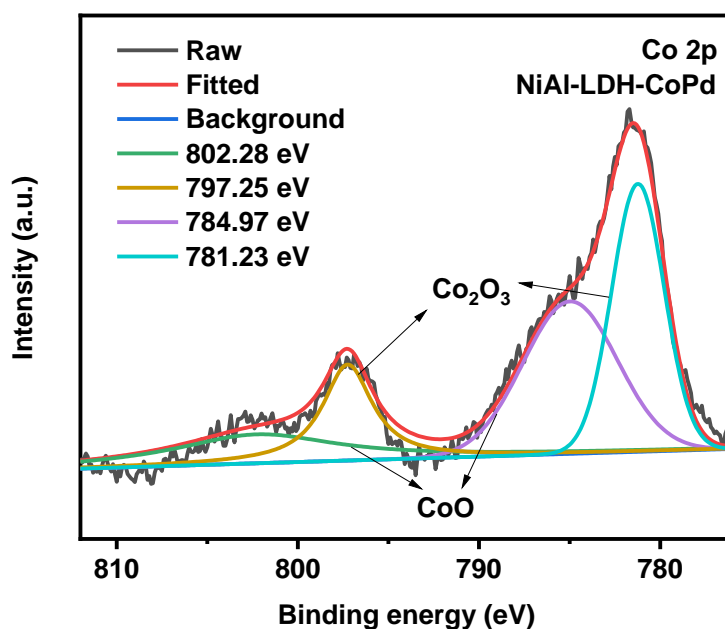


Fig. S8 High resolution XPS spectra of Co 2p in NiAl-LDH-CoPd.

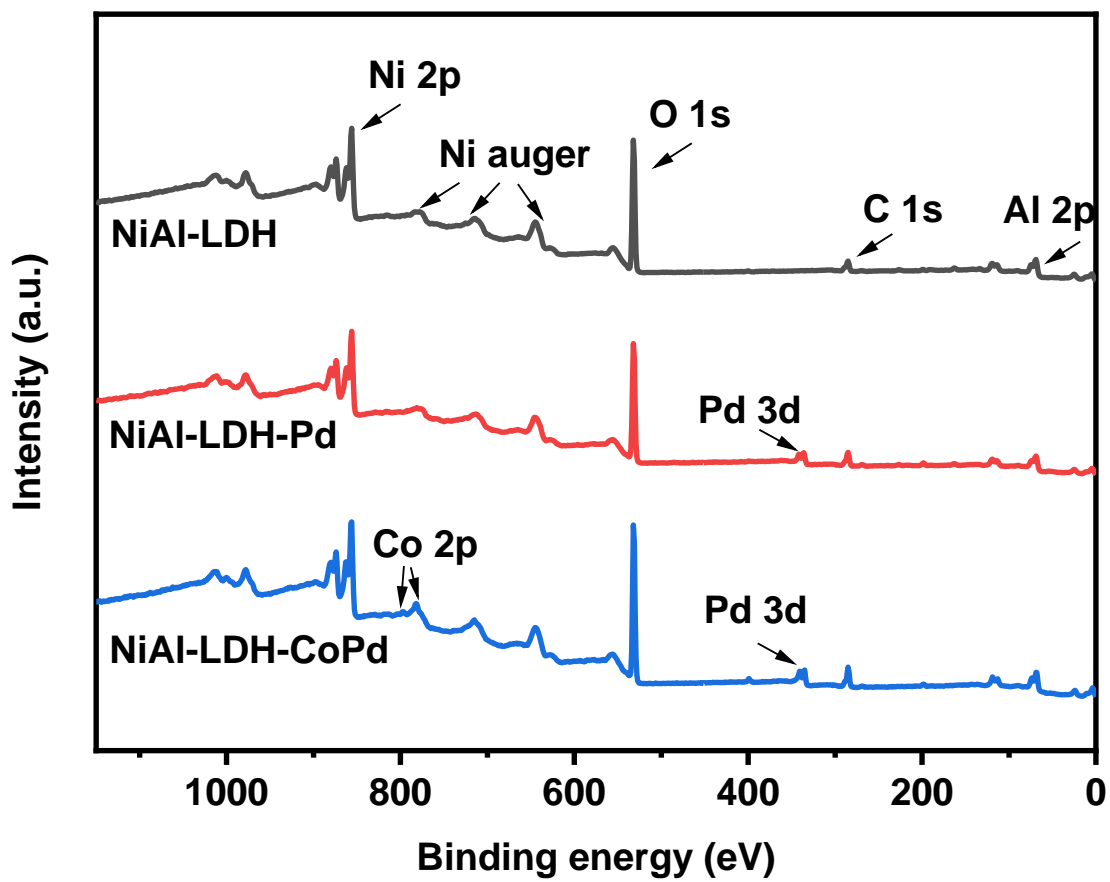


Fig. S9 XPS survey of NiAl-LDH, NiAl-LDH-Pd, and NiAl-LDH-CoPd.

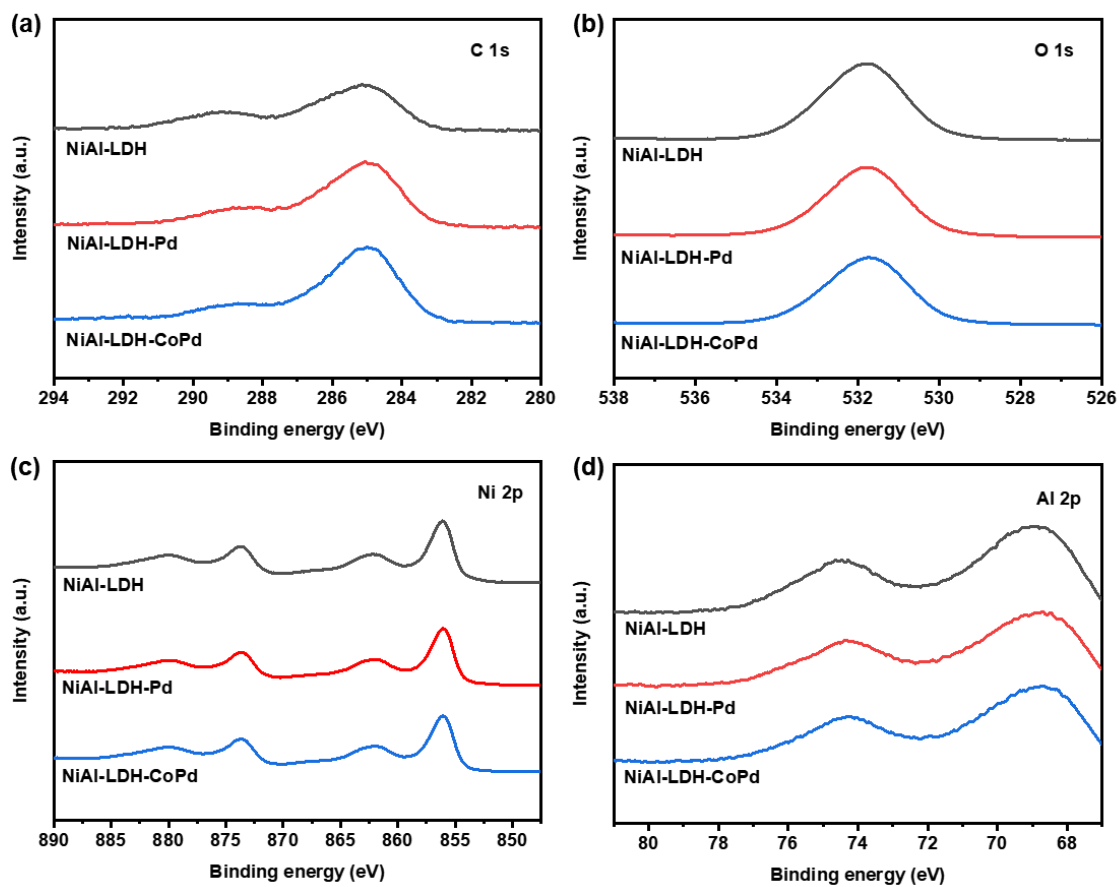


Fig. S10 High resolution XPS spectra of (a) C 1s; (b) O 1s; (c) Ni 2p; (d) Al 2p in NiAl-LDH, NiAl-LDH-Pd, and NiAl-LDH-CoPd.

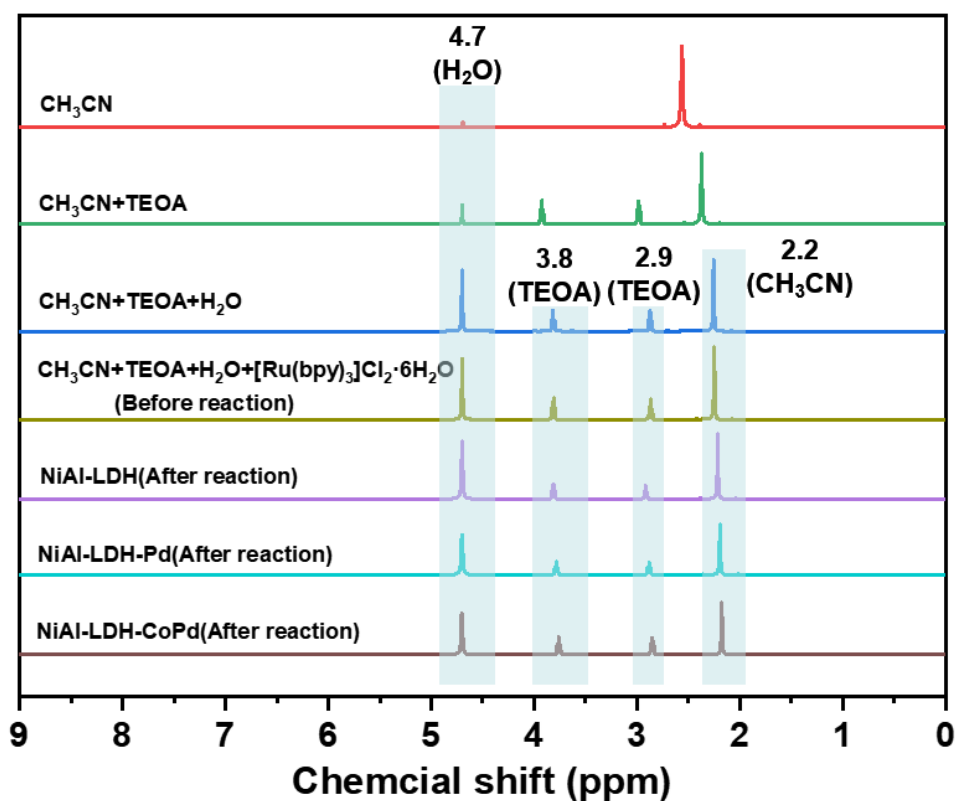


Fig. S11 $^1\text{H-NMR}$ spectra of liquid reactant taken from the reaction system (irradiating with $\lambda > 420$ nm for 1h).

D_2O was chosen as the deuterated reagent, so the peak at 4.7 ppm was the solvent residual peak of D_2O and the signal of H_2O in reaction system. According to the results of CH_3CN , the mixture of CH_3CN and TEOA, and the mixture of CH_3CN , TEOA and H_2O , the peaks at 3.8 ppm and 2.9 ppm were ascribed to TEOA, the peak at 2.2 ppm was the signal of CH_3CN . No new peaks presented after the addition of $[\text{Ru}(\text{bpy})_3]\text{Cl}_2 \cdot 6\text{H}_2\text{O}$. For NiAl-LDH, NiAl-LDH-Pd and NiAl-LDH-CoPd, the signals after reaction kept the same as that before reaction. The peaks of other liquid products in photocatalytic CO_2 reduction were not discovered.

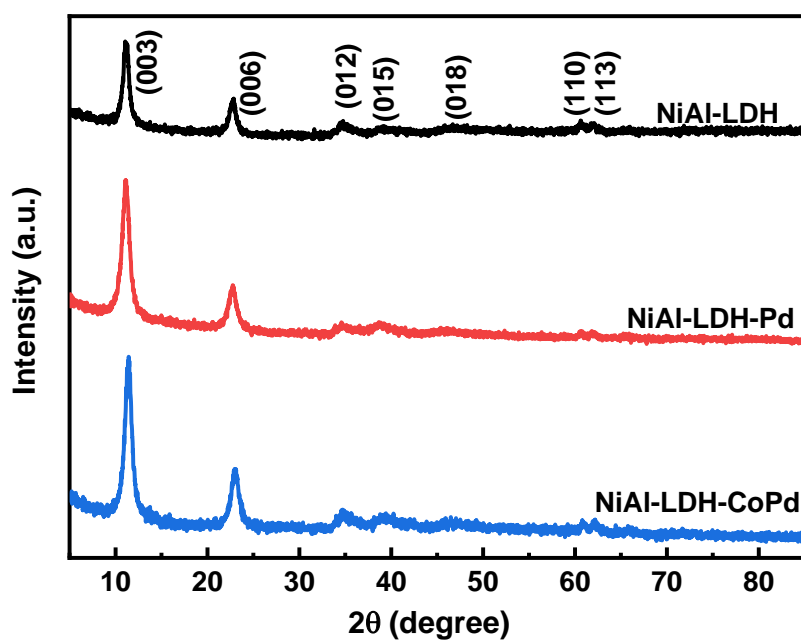


Fig. S12 The XRD pattern of samples after reaction.

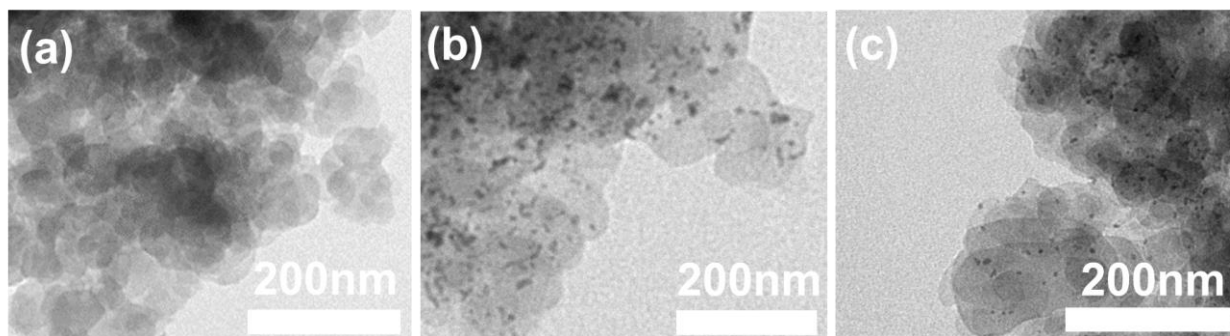


Fig. S13 TEM images of (a) NiAl-LDH, (b) NiAl-LDH-Pd, (c) NiAl-LDH-CoPd after reaction.

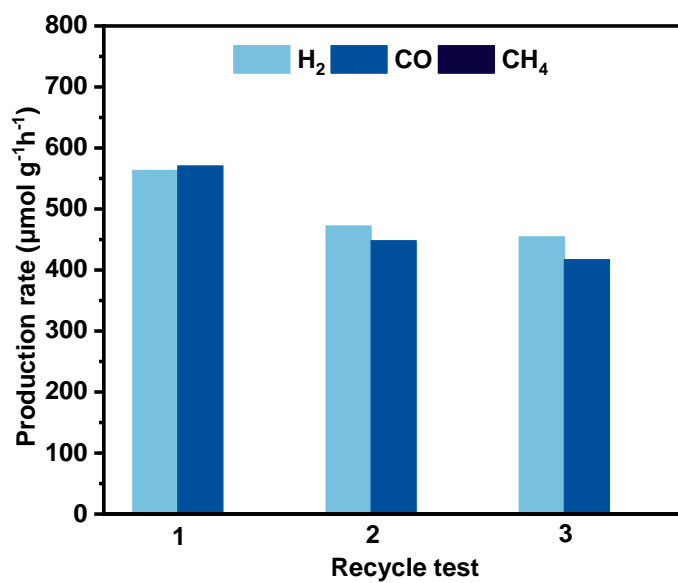


Fig. S14 The production rates of H₂, CO, and CH₄ in recycle test of NiAl-LDH-CoPd (irradiating with $\lambda > 420$ nm)

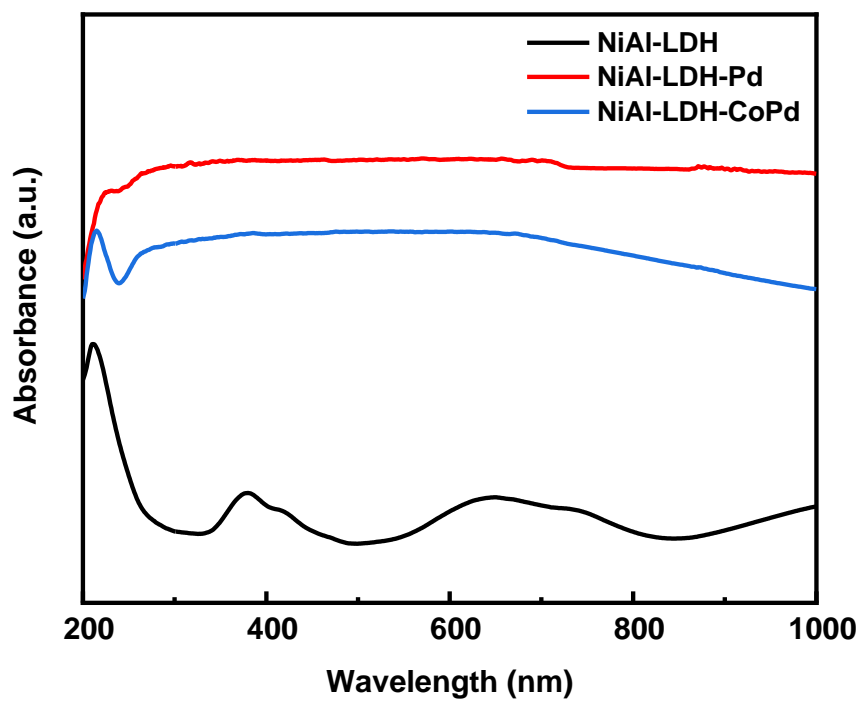


Fig. S15 UV-visible diffuse reflectance spectra (UV-vis) of the NiAl-LDH, NiAl-LDH-Pd, and NiAl-LDH-CoPd.

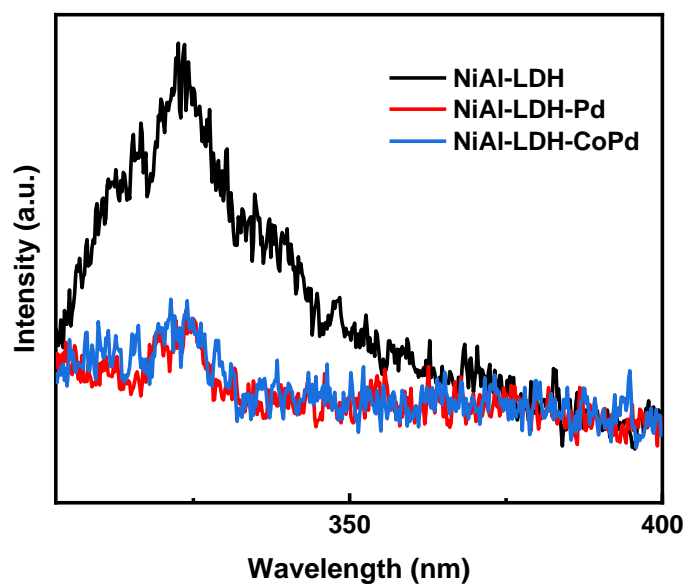


Fig. S16 PL spectra of NiAl-LDH, NiAl-LDH-Pd, and NiAl-LDH-CoPd excited at 280 nm

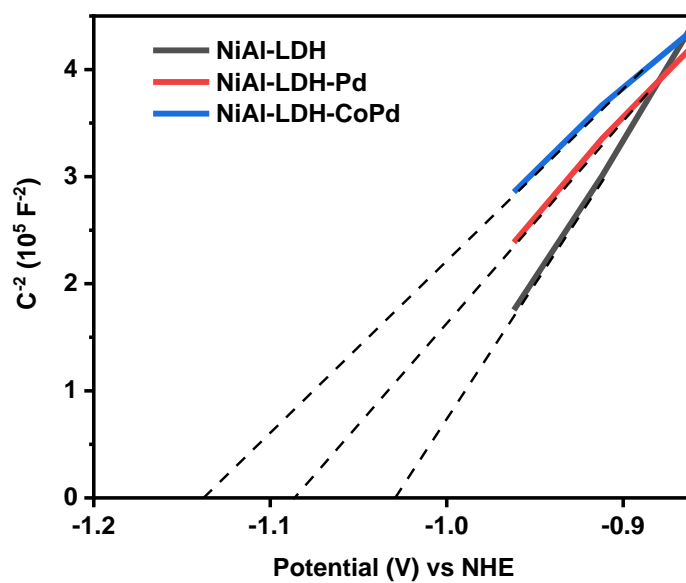


Fig. S17 Mott-Schottky plots of NiAl-LDH, NiAl-LDH-Pd, and NiAl-LDH-CoPd

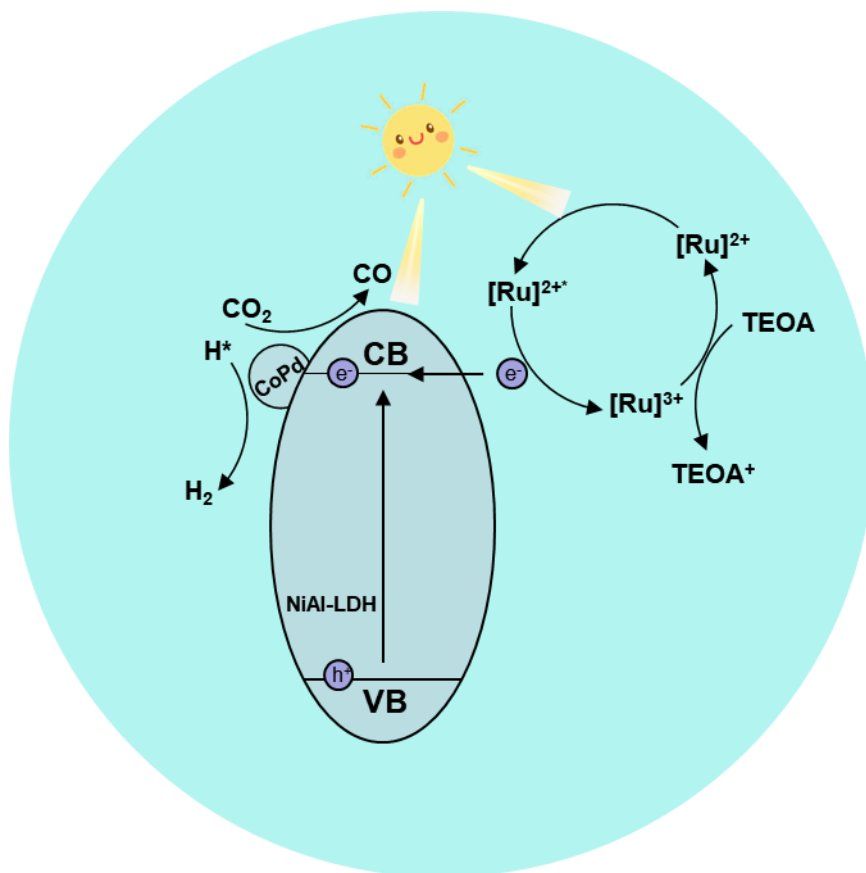


Fig. S18 The mechanism illustration of the photoreduction of CO₂ on NiAl-LDH-CoPd.

Tab. S1 The mass ratios of Co to Ni+Al and Pd to Ni+Al obtained from ICP-AES analysis.

Photocatalyst	Co/Ni+Al	Pd/Ni+Al
NiAl-LDH	-	-
NiAl-LDH-Pd	-	0.2082
NiAl-LDH-CoPd	0.0668	0.1346

Tab. S2 The apparent quantum yield (AQY) values of CO production and H₂ production for NiAl-LDH-CoPd under different approximate monochromatic wavelength irradiation.

Wavelength (nm)	AQY _{co} (%)	AQY _{H₂} (%)
420	0.087	0.115
450	0.025	0.032
475	0.097	0.102
500	0.023	0.032

Tab. S3 The photocatalytic CO₂ reduction performance of photocatalysts in this work and previous literature.

Photocatalyst	Photosensitizer + Sacrificial reagent + Solvent	Light source	Productivity ($\mu\text{molg}^{-1} \text{h}^{-1}$)	Reference
C-BN	CoCl ₂ 2'2-bipyridine + TEOA + H ₂ O	300 W Xe ($\lambda > 420\text{nm}$)	CO: 9.3 H ₂ : 2.9	Nature communications, 2015, 6(1): 1-7 ⁷
Co-ZIF-9	[Ru(bpy) ₃]Cl ₂ 6H ₂ O + TEOA + MeCN-H ₂ O(4:1 v/v)	300 W Xe ($\lambda > 420\text{nm}$)	CO: 41.8 H ₂ : 30.3	Angewandte Chemie, 2014, 126(4): 1052- 1056 ⁸
MAF-X27-OH	[Ru(bpy) ₃]Cl ₂ 6H ₂ O + TEOA + MeCN-H ₂ O(4:1 v/v)	300 W Xe ($\lambda > 420\text{nm}$)	CO: 45 H ₂ : 0.8	Journal of the American Chemical Society, 2018, 140(1): 38-41 ⁹
MnO _x @TiO ₂ @ CuPt	- + Na ₂ SO ₃ + H ₂ O	100 mW/cm ² AM 1.5G	CO: 84.2 H ₂ : 168.4	Chemical Science, 2018, 9(24): 5334- 5340 ¹⁰
Ru(Pd)- Au@SrTiO ₃	- + - + H ₂ O	300 W Xe ($\lambda > 400\text{nm}$)	CO: 369.2 H ₂ : 69.4 CH ₄ : 2.8	Chemical Communications, 2016, 52(35): 5989-5992 ¹¹
Co/C	[Ru(bpy) ₃]Cl ₂ 6H ₂ O + TEOA + MeCN-H ₂ O(4:1 v/v)	300 W Xe ($\lambda > 450\text{nm}$)	CO: 448 H ₂ : 250	Small, 2018, 14(33): 1800762. ¹²
CoAl-LDH	[Ru(bpy) ₃]Cl ₂ 6H ₂ O + TEOA + MeCN-H ₂ O(3:1 v/v)	300 W Xe ($\lambda > 400\text{nm}$)	CO: 2029.1 H ₂ : 1501.1	Journal of Energy Chemistry, 2020, 46: 1- 7 ¹³
Pd/CoAl-LDH- 7.57	[Ru(bpy) ₃]Cl ₂ 6H ₂ O + TEOA + MeCN-H ₂ O(3:1 v/v)	300 W Xe ($\lambda > 400\text{nm}$)	CO: 581.8 H ₂ : 1299.1	Journal of Energy Chemistry, 2020, 46: 1- 7 ¹³
NiAl-LDH	[Ru(bpy) ₃]Cl ₂ 6H ₂ O + TEOA + MeCN-H ₂ O(3:1 v/v)	300 W Xe ($\lambda > 420\text{nm}$)	CO: 275.0 H ₂ : 38.7	This work
NiAl-LDH-Pd	[Ru(bpy) ₃]Cl ₂ 6H ₂ O + TEOA + MeCN-H ₂ O(3:1 v/v)	300 W Xe ($\lambda > 420\text{nm}$)	CO: 102.7 H ₂ : 169.2	This work
NiAl-LDH-CoPd	[Ru(bpy) ₃]Cl ₂ 6H ₂ O + TEOA + MeCN-H ₂ O(3:1 v/v)	300 W Xe ($\lambda > 420\text{nm}$)	CO: 570.7 H ₂ : 563.1	This work

Notes and references

1. N. Iyi, Y. Ebina and T. Sasaki, *J. Mater. Chem.*, 2011, **21**, 8085-8095.
2. P. Li, W. Liu, J. S. Dennis and H. C. Zeng, *Adv. Funct. Mater.*, 2016, **26**, 5658-5668.
3. G. Kresse and J. Furthmüller, *Comput. Mater. Sci.*, 1996, **6**, 15-50.
4. P. E. Blöchl, *Phys. Rev. B*, 1994, **50**, 17953.
5. J. P. Perdew, J. A. Chevary, S. H. Vosko, K. A. Jackson, M. R. Pederson, D. J. Singh and C. Fiolhais, *Phys. Rev. B*, 1992, **46**, 6671.
6. H.-J. Oh, V.-D. Dao and H.-S. Choi, *J. Alloys Compd.*, 2017, **705**, 610-617.
7. C. Huang, C. Chen, M. Zhang, L. Lin, X. Ye, S. Lin, M. Antonietti and X. Wang, *Nat. Commun.*, 2015, **6**, 7698.
8. S. Wang, W. Yao, J. Lin, Z. Ding and X. Wang, *Angew. Chem. Int. Ed.*, 2014, **53**, 1034-1038.
9. Y. Wang, N. Y. Huang, J. Q. Shen, P. Q. Liao, X. M. Chen and J. P. Zhang, *J. Am. Chem. Soc.*, 2018, **140**, 38-41.
10. A. Li, T. Wang, X. Chang, Z. J. Zhao, C. Li, Z. Huang, P. Yang, G. Zhou and J. Gong, *Chem. Sci.*, 2018, **9**, 5334-5340.
11. D. Li, S. Ouyang, H. Xu, D. Lu, M. Zhao, X. Zhang and J. Ye, *Chem. Commun.*, 2016, **52**, 5989-5992.
12. K. Zhao, S. Zhao, C. Gao, J. Qi, H. Yin, D. Wei, M. F. Mideksa, X. Wang, Y. Gao, Z. Tang and R. Yu, *Small*, 2018, **14**, 1800762.
13. X. Wang, Z. Wang, Y. Bai, L. Tan, Y. Xu, X. Hao, J. Wang, A. H. Mahadi, Y. Zhao, L. Zheng and Y.-F. Song, *J. Energy Chem.*, 2020, **46**, 1-7.